communications physics

A Nature Portfolio journal

Article

https://doi.org/10.1038/s42005-026-02578-8

Tunable field-linked *s*-wave interactions in dipolar fermi mixtures

Jing-Lun Li [1] ✉, Georgios M. Koutentakis [1], Mateja Hrast [1], Mikhail Lemeshko[1], Andreas Schindewolf [2] & Ragheed Alhyder [1] ✉

Spin mixtures of degenerate fermions are a cornerstone of quantum many-body physics, enabling superfluidity, polarons, and rich spin dynamics through *s*-wave scattering resonances. Combining them with strong, long-range dipolar interactions provides highly flexible control schemes promising even more exotic quantum phases. Recently, microwave shielding gave access to spin-polarized degenerate samples of dipolar fermionic molecules, where tunable *p*-wave interactions were enabled by field-linked resonances available only by compromising the shielding (due to experimental limitations). Here, we study the scattering properties of a fermionic dipolar spin mixture and show that a universal *s*-wave resonance is readily accessible without compromising the shielding. We develop a universal description of the tunable *s*-wave interaction and weakly bound tetratomic states based on the microwave-field parameters. The *s*-wave resonance paves the way to stable, controllable and strongly-interacting dipolar spin mixtures of deeply degenerate fermions and supports favorable conditions to reach this regime via evaporative cooling.

Ultracold fermionic mixtures provide a powerful platform for studying strongly interacting quantum matter[1,2]. Their ability to scatter through *s*-wave collisions underpins efficient thermalization, evaporative cooling, and the emergence of superfluidity at low temperatures[3]. The ability to tune interactions in atomic mixtures via magnetic Feshbach resonances[4] has led to landmark discoveries, including the BCS–BEC crossover and universal dynamics near unitarity[5]. Building on these advances, the incorporation of long-range dipolar interactions offers exciting prospects, from anisotropic superfluids[6] to quantum spin liquids[7] and topological phases[8]. Ultracold dipolar fermionic spin mixtures have been realized using atomic species with large magnetic moments[9]. The dipole–dipole interaction is, in this case, however, quite small and every state has a different magnetic dipole moment. In contrast, ultracold molecules with electric dipole moments offer strong, long-range dipole–dipole interactions and a rich internal structure[10–14]. This makes them ideal for exploring many-body physics and exotic quantum phases,[15–18], and the spin properties of the inter-molecular interaction offer the potential for realizing the SU(N) symmetry[19,20]. Therefore, it is highly desirable to explore the tunability of the interaction provided by such molecular systems.

However, dipolar gases also bring new challenges: on one side, the attractive part of the dipole–dipole interaction enhances inelastic collisions and induces collapses[21,22]; on the other side, ultracold molecules undergo inelastic processes in short-range collisions through chemical reactions or sticky complex formation[23–28], complicating the route to deeply degenerate, stable mixtures. This limits the implementation of magnetic Feshbach resonances, the traditional tool for tuning the inter-molecular interactions, which are accessible only in specific molecular systems[29] and require access to short-range tetratomic states. A powerful tool to overcome this challenge, the so-called microwave shielding, has recently emerged through microwave dressing of polar molecules. By coupling the rotational ground state to the first excited manifold with a blue-detuned circularly or elliptically polarized microwave field, an avoided crossing forms in the inter-molecular potential landscape, resulting in a field-induced barrier that dramatically suppresses inelastic losses at short range[11,30–36]. This further enables the tuning of the scattering properties through coupling to field-linked bound states that emerge in the interaction potential for suitable field parameters[11,32,34,37–46]. Microwave shielding has recently led to the creation of a stable degenerate dipolar Fermi gas[47], and later this method was extended to dual-microwave shielding[48,49], which enabled the creation of the first Bose–Einstein condensates of dipolar molecules[50,51].

So far, microwave shielding has been restricted to gases composed of a single internal state. In the fermionic system, collisions occur primarily via *p*-wave channels. While enhanced *p*-wave interactions have recently been demonstrated by tuning to a field-linked resonance (FLR)[42], this required a highly elliptical field polarization, which compromises the shielding efficiency and thereby the stability of the sample[52]. The fermionic systems with the lowest entropy ($T/T_F \simeq 0.36$[47], where T_F is the Fermi temperature) have therefore been prepared far away from an FLR.

[1]Institute of Science and Technology Austria (ISTA), Am Campus 1, 3400 Klosterneuburg, Austria. [2]Vienna Center for Quantum Science and Technology, Atominstitut, TU Wien, Stadionallee 2, 1020 Vienna, Austria. ✉e-mail: jinglun.li@ist.ac.at; Ragheed.AlHyder@ist.ac.at

Here, we show that introducing a second spin state naturally provides tunable *s*-wave interactions in the experimentally accessible parameter regime with circular microwave polarization, i.e., without compromising the stability of the system through elliptical polarization. We solve the coupled-channel scattering problem between two microwave-dressed molecules in different spin states, with a restriction of the molecular rotational motion to the ground and first-excited manifolds. We find that the scattering length can be steered from strongly attractive to strongly repulsive by adjusting the microwave field parameters around an FLR. This FLR exhibits universal behavior in terms of the field-linked parameters, persisting across different molecular species[53]. This universality enables the prediction of *s*-wave scattering properties and weakly bound states via simple expressions. The combination of fermionic statistics, the absence of ellipticity and deeper bound states provides favorable conditions for a stable, strongly-interacting and highly-tunable dipolar spin mixture. This universality enables the estimate of FLR positions and widths in a wide range of field parameters via a simple expression.

Results

Two-molecule scattering setup

We construct the two-body problem starting from the microwave-dressed single-molecule Hamiltonian that couples the $J = 0$ and $J = 1$ rotational manifolds. In the co-rotating frame the field produces four dressed states $\{|+\rangle, |-\rangle, |0\rangle, |\xi^-\rangle\}$ whose energies depend only on the control parameters. These consist of Ω, the microwave Rabi frequency (coupling strength), δ, the detuning from the $J = 1$ rotational state, and ξ, the ellipticity of the field polarization (see Methods), which here is considered circular ($\xi = 0$). The molecules are prepared in the $|+\rangle$ state, leading to an anisotropic adiabatic interaction potential $V^{++}(r, \theta)$ with a strongly repulsive core (the shielding potential) in the two-molecule $|++\rangle$ state, depicted in Fig. 1(a). In the case of fermionic molecules, the internal spin state plays a crucial role in their scattering properties. In particular, two molecules with unlike spin states, i.e. different nuclear spins (see Methods), can collide in the *s*-wave channel of the shielding potential (V_s^{++} in Fig. 1(a)). In contrast, in the case of identical spin states, the lowest collisional channels have *p*-wave character (V_{p0}^{++},V_{p1}^{++} and V_{p-1}^{++}, see also Methods).

By tuning the microwave field parameters, one can introduce a FLR associated with a weakly bound tetratomic state (dimer state of two diatomic molecules). As shown in Fig. 1(b), in the vicinity of the *s*-wave FLR, the scattering length characterising the inter-spin interaction is significantly enhanced while the intra-spin *p*-wave interaction remains almost unchanged, since the *p*-wave FLR is located ~ 60 MHz away. This provides a flexible way to selectively control inter- and intra-spin interactions and scattering dynamics.

In the following, we focus on fermionic $^{23}Na^{40}K$ molecules, which have been employed in previous experimental studies[42,44,47]. However, our results are universal and can be applied to other species for $\delta \ll B_{\rm rot}/\hbar$ and $\Omega \ll B_{\rm rot}/\hbar$[53], where $B_{\rm rot}$ denotes the molecular rotational constant (see Methods). Our interaction Hamiltonian contains the electric dipole–dipole coupling within the rotating-wave approximation (RWA), van der Waals interactions, and an absorbing short-range boundary condition. Coupled-channel equations are solved, yielding elastic and inelastic scattering matrices, from which all scattering observables follow (for numerical details see Methods and Supplementary Note 1). We present in the following a full characterisation of the FLRs, providing a simple expression for the scattering length, the position of the FLR, its width, and the weakly bound tetratomic state. Afterwards, we delve deeper into the scattering properties and the various enhancements FLRs can bring to experimental setups.

Universal characterisation of *s*-wave field-linked resonances and tetratomic molecules

We study the FLR by computing the *s*-wave scattering length at zero collisional energy limit while sweeping the microwave coupling strength Ω. We find divergences reminiscent of Feshbach resonances in atomic physics (see Fig. 1(b)), which grant precise and tunable control over the *s*-wave interaction strength.

To characterise FLRs, we fit the calculated *s*-wave scattering length α_s (real part) to the following form:

$$\alpha_s = \alpha_{\rm sbg}\left(1 + \sum_i \frac{\Delta_i}{\Omega - \Omega_{{\rm r}_i}}\right) + b\,\Omega, \tag{1}$$

where $\alpha_{\rm sbg}$ denotes the background scattering length, $\Omega_{{\rm r}_i}$ and Δ_i are the position and width of the *i*th FLR, respectively. The imaginary part of the scattering length is typically several orders of magnitude smaller than the real part (see Supplementary Note 2), and we therefore neglect it in our analysis. In practice, we run a focused scan of $\Omega \in 2\pi \times [0, 100]$ MHz for addressing the first FLR or a wide scan of $\Omega \in 2\pi \times [0, 800]$ MHz for addressing the first two FLRs, by fitting the resulting scattering length for $|\delta|/\Omega = 0$, as exemplified in Fig. 2(a). We extract the resonance positions $\Omega_{{\rm r}_i}$, background scattering length $\alpha_{\rm sbg}$, the linear coefficient b, and the effective widths $\bar{\Delta}_i \equiv \alpha_{\rm sbg}\Delta_i$, defined to improve the numerical stability of the fit. We then proceed to fit the FLRs at various fixed $|\delta|/\Omega \in [0, 1]$ to explore their control via field parameters (Fig. 2(b), (c)).

For a given value of the detuning $|\delta|/\Omega$, the fitted background scattering length $\alpha_{\rm sbg}$ depends strongly on the scan range of Ω (see Supplementary Note 3). The observed variation in $\alpha_{\rm sbg}$ is remedied by incorporating the next-to-leading linear term ($b\,\Omega$ in Eq. (1)) to achieve good fitting quality. We find that the inclusion of the linear correction helps to reproduce the resonance shape of the FLR. We attribute this feature to the existence of higher resonances for larger field strengths and to the fact that the interaction takes place on a single potential curve reshaped by the microwave field, leading to a varying background scattering length. In contrast, for magnetically tuned Feshbach resonances[4], $\alpha_{\rm sbg}$ is fixed by the open channel parameters for a given atomic or molecular species. Note that the fit does not work for low Ω ($< 2\pi \times 10$ MHz), but in this regime there exist strong losses due to inefficient shielding. Crucially, the fitted positions and widths of the FLR remain stable if we change the scan range of Ω (see Supplementary Note 3).

The field dependence of the resonance position $\Omega_{{\rm r}_i}$ and effective width $\bar{\Delta}_i$ is governed by the long-range $-C_4/r^4$ potential, with $C_4 = d^4 m/[\hbar^2 1080(4\pi\epsilon_0)^2(1 + (\delta/\Omega)^2)^2]$ for microwave dressed molecules[54] (see also Supplementary Note 4), where d denotes the molecule's permanent dipole moment and ϵ_0 is the vacuum permittivity. In the asymptotic region $r \gg R_4$, this potential dominates the inter-molecular interactions, and defines the characteristic length $R_4 = (mC_4)^{1/2} \propto (1 + (|\delta|/\Omega)^2)^{-1}$ and energy $E_4 = \hbar^2/mR_4^2 \propto (1 + (|\delta|/\Omega)^2)^2$ scales. For a pure $-C_4/r^4$ potential, one finds $\Omega_{{\rm r}_i} \propto E_4$ and $\Delta_i \propto R_4 E_4$ (see Supplementary Note 4), thus both quantities for the first ($i = 1$) and second ($i = 2$) FLRs increase with $|\delta|/\Omega$ as observed in Fig. 2(b), (c). However, at intermediate and short-ranges, the $-C_4/r^4$ potential will be modified by the repulsive core of the adiabatic shielding potential and other forces. Hereafter, we use the term short-range specifically to describe the repulsive core of the adiabatic shielding potential (typically located at a few hundred a_0), which should not be confused with the regime of electron exchange (typically on the order of 10 a_0).

Consequently, to describe the increasing behaviour of $\Omega_{{\rm r}_i}$ and $\bar{\Delta}_i$, we derive the following simple relations (see Supplementary Note 4)

$$\Omega_{{\rm r}_i} = c_{\Omega_{\rm r}}[1 + \lambda_{\Omega_{\rm r}}(|\delta|/\Omega)^2]^2, \tag{2}$$

$$\bar{\Delta}_i = c_\Delta[1 + \lambda_\Delta(|\delta|/\Omega)^2], \tag{3}$$

which we use as fitting functions in Fig. 2(b), (c). Here, $c_{\Omega_{\rm r}}$, c_Δ are the scaling coefficients and $\lambda_{\Omega_{\rm r}}$, $\lambda_\Delta \neq 1$ represent short-range correction terms to the scaling, accounting for deviations from the $-C_4/r^4$ potential for $\Omega_{{\rm r}_i}$, $\bar{\Delta}_i$, respectively.

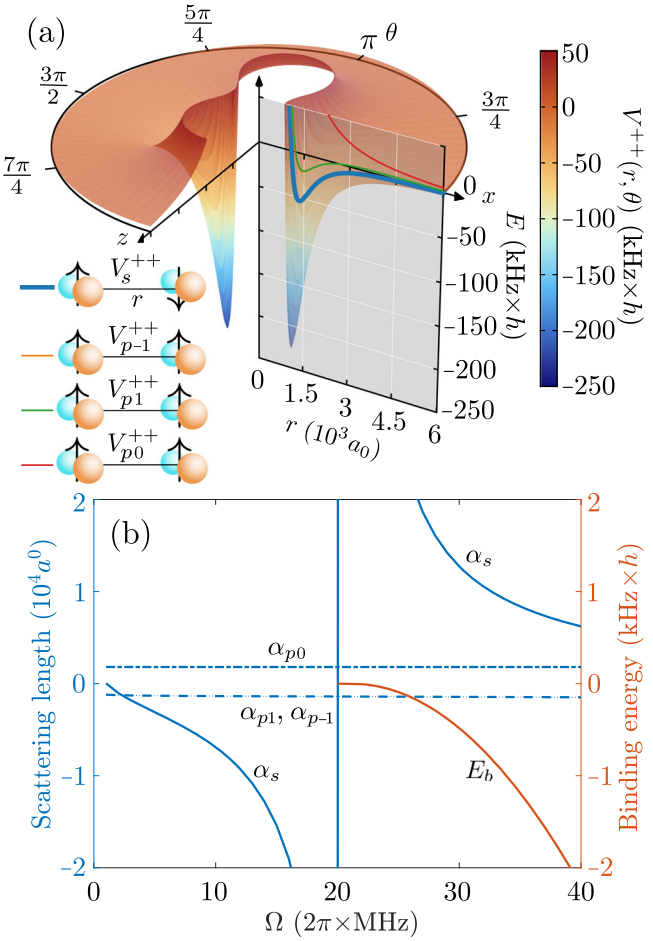

Fig. 1 | Inter- and intra-molecular scattering properties of the two-component fermionic molecular gas. a Potential energy surface, $V^{++}(r, \theta)$ of the $|{+}{+}\rangle$ collisional dressed state of microwave shielded molecules. The potential energy curves of s-wave $V_s^{++}(r)$ and p-wave $V_{pm_p}^{++}(r)$ channels, corresponding to unlike and like spins, respectively, are also provided. We note that the curves of $V_{p1}^{++}(r)$ and $V_{p-1}^{++}(r)$ are overlaped. In all cases ^{23}Na^{40}K was considered with $\Omega = 2\pi \times 21$ MHz and $\delta = 0$. **b** Inter- and intra-spin interactions characterised by the s-wave scattering length α_s and the energy-dependent p-wave scattering length $\alpha_{pm_p}(k)$, respectively, obtained at $\delta = 0$. The binding energy E_b of the s-wave weakly bound tetratomic state is also displayed. The energy-dependent p-wave scattering length is calculated at $E = 21$ nK, achieved in a previous experiment[47]. In the unit, a_0 denotes the Bohr radius.

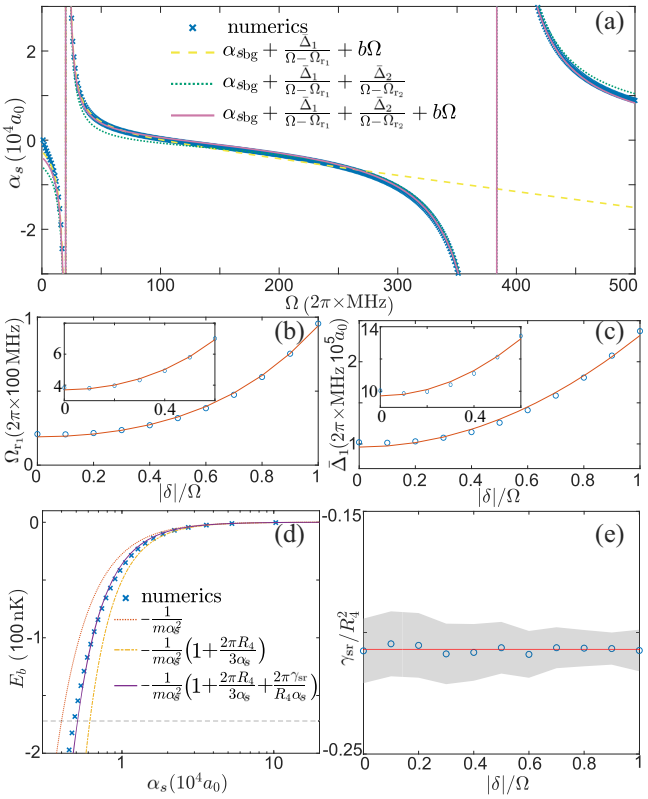

Fig. 2 | Universalities of two-molecule scattering and bound states. a Scattering length versus microwave coupling strength at fixed $|\delta|/\Omega = 0$ shows the first and second FLRs. The cross symbols represent numerical calculations, while the lines denote the fitting results. **b**, **c** The position Ω_{r_1} and effective width Δ_1 of the first FLR increase with an increasing $|\delta|/\Omega$, respectively. The insets show the corresponding result for the second FLR. The solid lines in (**b**) and (**c**) the best fitting to Eqs (2) and (3). Panel (**d**) displays the binding energy of the weakly bound tetratomic state versus scattering length at $\delta/\Omega = 0$, in the vicinity of the first FLR. The symbols represent the numerical calculation, while dotted and dashed lines indicate the universal formula to the order of $1/\alpha_s^2$ and $1/\alpha_s^3$ respectively. The solid line denotes the best fit to the $1/\alpha_s^3$ order, including the short-range correction parameter γ_{sr}. **e** The scaled short-range parameters γ_{sr}/R_4^2 versus $|\delta|/\Omega$ for the first FLR. The grey area indicates the 95% confidence interval from the fitting. The red solid denotes the mean value of $\gamma_{sr}/R_4^2 = -0.21$.

The scaling coefficients and short-range correction parameters are extracted by fitting Eqs. (2) and (3) and are summerized in Table 1. We observe that both coefficients for the resonance position c_{Ω_r} and the width c_Δ increase significantly from the first to the second FLR, indicating that the latter (occurring at a much higher microwave coupling strength) becomes considerably broader. For the first FLR, the short-range correction factors deviate from unity ($\lambda_{\Omega_r} = 1.22$ and $\lambda_\Delta = 1.41$), reflecting a non-negligible contribution from the short-range interaction. In contrast, the second FLR yields $\lambda_{\Omega_r} \simeq 1$ and $\lambda_\Delta \simeq 1$, indicating that short-range contributions are negligible. This trend arises because the larger Rabi frequency, at which the second FLR appears, pushes the repulsive barrier to smaller inter-molecular separations, thereby enhancing the role of the long-range $-C_4/r^4$ potential and limiting the short-range contribution. As a result, observables exhibit nearly universal scaling with R_4 and E_4 in the vicinity of the second FLR. Similarly, this universality is expected to persist for higher FLRs when $\Omega \ll B_{\rm rot}/\hbar$.

A different universal behavior has recently been demonstrated in identical bosonic and fermionic dipolar molecules[53], where the properly rescaled scattering quantities are identical across different species for a given $|\delta|/\Omega$, when $\delta \ll B_{\rm rot}/\hbar$ and $\Omega \ll B_{\rm rot}/\hbar$. We verify that such a species-based universality can be generalized to include two-component fermionic dipolar molecules (see Supplementary Note 2), complementing the field-based ($|\delta|/\Omega$-based) universality we find for the second (and higher) FLRs for a given molecular species. In practice, using the parameters from Table 1, our simple expressions (2) and (3) provide an easy-to-use tool for estimating the scattering length in the vicinity of the first two FLRs of the two-component ^{23}Na^{40}K molecular species. This formalism is generally applicable to other two-component fermionic or identical bosonic dipolar molecules when incorporated with the species-based universality, by using the values of the rescaled $\widetilde{c}_{\Omega_r}$ and $\widetilde{c}_\Delta$ coefficients in Table 1 in combination with the length ($R_3 = md^2/\hbar^2 4\pi\epsilon_0$) and energy ($E_3 = \hbar^2/mR_3^2$) scales of dipole-dipole interaction. We have demonstrated this applicability by using ^{23}Na^{87}Rb as an example (see Supplementary Note 2). As a result, our characterization of the second (and higher) FLR, currently inaccessible to state-of-the-art experiments of ^{23}Na^{40}K, can still be experimentally relevant for a molecular species with a smaller E_3. We note that the validity range of the field-based universality is expected to be as $\delta \ll B_{\rm rot}/\hbar$ and $\Omega \ll B_{\rm rot}/\hbar$, where the species-based universality holds[53]. These conditions are not fully satisfied at the second FLR of ^{23}Na^{40}K. However, the species-relevant nonuniversal contribution ($\propto \Omega/B_{\rm rot}$[53]) is neglected in our model in order to solely focus on the universal scattering properties.

Table 1 | The fitted coefficients ($c_{\Omega_r}, c_\Delta, \lambda_{\Omega_r}, \lambda_\Delta$) of position and width of the first (FLR1) and second (FLR2) FLRs

	c_{Ω_r}	$\tilde{c}_{\Omega_r}$	c_Δ	$\tilde{c}_\Delta$	λ_{Ω_r}	λ_Δ
FLR1	19.11 (0.99)	5.76×10^6	9.61(0.40)	2.20×10^5	1.22 (0.07)	1.41(0.14)
FLR2	369.5 (12.3)	1.11×10^8	97.11(3.01)	2.23×10^6	1.03(0.09)	1.01(0.20)

The values of c_{Ω_r} and c_Δ are in $2\pi \times$ MHz and $2\pi \times$ MHz $10^4 a_0$, respectively. To generalize the results to other species, the dimensionless coefficients are introduced by scaling c_{Ω_r} and c_Δ as $\tilde{c}_{\Omega_r} = \hbar c_{\Omega_r}/E_3$ and $\tilde{c}_\Delta = \hbar c_\Delta/E_3 R_3$. The values of $\tilde{c}_{\Omega_r}$ and $\tilde{c}_\Delta$ are also listed (without error bar). Here $R_3 = m d^2/\hbar^2 4\pi\epsilon_0$ and $E_3 = \hbar^2/m R_3^2$ are the chracteristic length and energy scales of the dipole–dipole interaction, respectively[53,76].

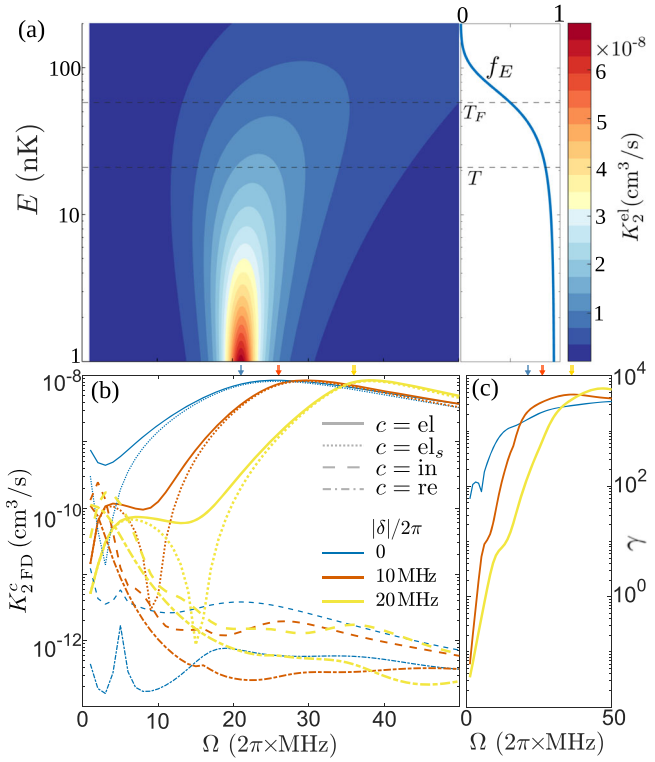

Fig. 3 | Two-molecule elastic and inelastic scattering analysis. a Left panel: elastic scattering rate $K_2^{\rm el}$ versus microwave coupling strength Ω and collisional energy E at fixed detuning $\delta = 0$. Right panel: Fermi–Dirac distribution f_E with $T = 21$ nK, $T_F = 58$ nK and $\bar{\omega} = 2\pi \times 60$ Hz, the typical experimental condition[47]. **b** Thermal averaged elastic (solid lines), inelastic (dashed lines), and reactive (dash-dotted lines) scattering rate ($K_{2\rm FD}^{\rm el}$, $K_{2\rm FD}^{\rm in}$, and $K_{2\rm FD}^{\rm re}$) considering f_E from the right panel of (**a**). The dotted lines denote $K_{2\rm FD}^{{\rm el}_s}$ the s-wave contribution to the elastic scattering rate. The detunings are $|\delta|/2\pi = 0$, 10 and 20MHz from thin to thick lines. **c** The ratio $\gamma = K_{2\rm FD}^{\rm el}/(K_{2\rm FD}^{\rm in} + K_{2\rm FD}^{\rm re})$ extracted from the result of (**b**). The arrows in (**b**) and (**c**) indicate the FLR positions at zero temperature.

In the following, we shall show that the field-linked tetratomic binding energy E_b depends universally on the scattering length and R_4, up to energies on the order of $E_b \sim -E_4$, allowing our universal framework to be extended to estimate the field-linked tetratomic molecular binding energy. Due to two-body loss, the field-linked tetratomic molecule can naturally dissociate through lower lying dressed states, which is expressed as a complex binding energy. For the two-component ^{23}Na^{40}K considered in this work, however, we find that this state is relatively long-lived, corresponding to a very small imaginary component of E_b (see Supplementary Note 5). We therefore neglect the imaginary part hereinafter.

To characterise the binding energy E_b of a weakly bound field-linked tetratomic state, we employ the quantization function $F_4(E)$ of the long-range $-C_4/r^4$ potential[55], supplemented by a short-range correction $\gamma_{\rm sr} mE/\hbar^2$ (see Supplementary Note 6). At $E = E_b$, the quantization function is related to the scattering length α_s via $\alpha_s = R_4/\tan[\pi F_4(E_b)]$. By solving for E_b from and expanding the solution to third order in $1/\alpha$ we find

$$E_b = -\frac{\hbar^2}{m\alpha_s^2}\left(1 + \frac{2\pi R_4}{3\alpha_s} + \frac{2\pi\gamma_{\rm sr}}{R_4\alpha_s}\right). \tag{4}$$

In Eq. (4), the $1/\alpha_s^3$ terms supply, respectively, the leading long-range and short-range corrections to the universal relation $E_b = -\hbar^2/(m\alpha_s^2)$. We note that for a pure $-C_4/r^4$ potential, the R_4 term has been introduced in a previous study[56], while the $\gamma_{\rm sr}$ term is derived here to describe the field-linked resonances. In Fig. 2(d), we find that the universal relation is valid only when $|E_b| \ll E_4$, while for larger E_b, it underestimates the exact energy, while the long-range correction overestimates it. Including the short-range term restores quantitative agreement up to $|E_b| \approx E_4$ as is demonstrated in Fig. 2(d). In addition, we find that the short-range parameter $\gamma_{\rm sr}$ normalized by R_4^2 is quite universal, for instance, $\gamma_{\rm sr}/R_4^2 \approx -0.21$ for the first FLR, as is shown in Fig. 2(e). Hence, Eq. (4) provides a practical and universal estimation of the field-linked binding energy estimated from α and R_4 in the regime $E_b \lesssim -E_4$. For higher FLRs, the universal value of $\gamma_{\rm sr}/R_4^2$ is expected to be much smaller.

Collisional landscape: elastic scattering and loss processes

In the vicinity of the FLR, the scattering length, and consequently the elastic scattering rate $K_2^{\rm el}$, is significantly enhanced. Figure 3(a) shows that, at zero detuning ($\delta = 0$), tuning the microwave coupling strength to $\Omega \simeq 2\pi \times 20$ MHz boosts the elastic rate by nearly an order of magnitude over a broad collision-energy interval $E \in [1, 200]$ nK. This enhancement becomes narrower in Ω but grows in amplitude as E is lowered, which is the desired behaviour for efficient evaporative cooling where colder molecules experience a higher probability of re-thermalising collisions once the high-energy tail is removed. Incorporating the Fermi-Dirac distribution in typical experimental conditions[47], the elastic scattering rate approaches the s-wave unitary limit 8.5×10^{-9} cm^3/s in the Ω range of $2\pi \times [20, 30]$ MHz, as is shown in Fig. 3(b).

The same calculation indicates that unfavorable inelastic and reactive scattering remain suppressed ($<10^{-11}$ cm^3/s and $< 10^{-12}$ cm^3/s, respectively), these are collisions that either scatter the molecules into other internal channels, or enter the regime where collisional complexes are formed within the repulsive core, respectively. This leads to the ratio $\gamma \equiv K_{2\rm FD}^{\rm el}/(K_{2\rm FD}^{\rm in} + K_{2\rm FD}^{\rm re})$ of the favorable to unfavorable collisions to be $\gamma > 10^3$, as is shown Fig. 3(c), which is suitable for evaporative cooling[33,34]. Close to the FLR, the elastic cross section is dominated by the isotropic s-wave component (as shown in Fig. 3(b)), which in addition to maximising $K_2^{\rm el}$, facilitates rapid cross-dimensional thermalisation[57–59], beyond what is achievable with intra-spin p-wave interactions[47]. Away from the FLR, higher partial waves do contribute and can even dominate under some conditions. Increasing $|\delta|$ shifts the FLR to larger Ω, where the suppression of losses is even stronger, leading to a larger γ. We note that the possible three-body recombination loss, which is encountered with NaCs[60,61], can be excluded on the $\alpha_s < 0$ side of the first FLR due to the absence of field-linked tetratomic (dimer) states. While a weakly-bound tetratomic state exists on the $\alpha_s > 0$ side, it does not cause particle loss when the binding energy is smaller than the depth of the trap. When the binding energy exceeds the trap depth, the dimer state can lead to three-body recombination. However, the associated loss rate L_3 is

expected to be suppressed at low temperatures ($L_3 \propto E$) by the three-body centrifugal barrier[62,63].

A further practical benefit is that the onset of strong interactions occurs at comparatively low and experimentally available microwave field strengths, obviating the need for elliptically polarized dressing fields[42,44] or extreme electric bias fields often required in static-dipole schemes[64]. This lower technical threshold simplifies experimental implementation and reduces residual heating typically presents due to inefficient shielding[65]. In addition, high elastic scattering rates at reasonable microwave field strengths are key in view of microwave phase noise that induces effective single-body decay and that becomes more severe at larger field strengths[47]. All these benefits facilitate evaporation to deeper degeneracy. Since the elastic scattering rate and the density of states grow as the gas cools, the elastic collision rate actually increases as the sample approaches quantum degeneracy. Consequently, the combination of a large K_2^{el}, a high γ, and favourable isotropic s-wave symmetry allows the system to cross into the degenerate regime at higher absolute temperatures and in shorter evaporation cycles than would be possible with p-wave interaction.

Finally, the enhanced scattering length pushes the system into the unitary-limited interaction regime for $|\alpha_s| \gtrsim k_F^{-1}$, where k_F is the Fermi momentum. This increases the many-body pairing gap and hence the superfluid transition temperature T_c relative to weak-coupling estimates[66], facilitating further cooling of the gas into the degenerate regime. Because the resonance occurs at $\Omega \ll B_{\mathrm{rot}}/\hbar$, the microwave dressing leaves rotational coherence intact, minimising decoherence-induced heating and making the FLR an attractive route towards efficient evaporation and strongly interacting dipolar Fermi superfluids.

The result above is obtained by considering $\xi = 0$. In practice, small but finite residual microwave ellipticities are inevitable, and in modern setups they can typically be limited to $\xi < 2°$ [44,67,68]. Our main conclusion remains unchanged within this level of ellipticity uncertainty (see Supplementary Note 5).

Conclusion

We have presented a comprehensive characterization of s-wave interactions and weakly bound tetratomic molecular states tuned by microwave field-linked resonances of fermionic dipolar spin-mixtures. Starting from the microwave-dressed Hamiltonian for two molecules with different spin states, we performed coupled-channel scattering calculations. The extracted s-wave resonance properties largely follow universal scalings that depend solely on the microwave field parameters. We derive simple universal expressions for the resonance position, width, and binding energy, and demonstrate that they remain accurate across a wide parameter range. Moreover, the resonance parameters of higher-order field-linked resonances were shown to be increasingly universal, manifested by vanishing short-range corrections. We refer to this universal behavior as the field-based universality, which is complemented by the recently introduced species-based universality[53], provided $\delta \ll B_{\mathrm{rot}}/\hbar$ and $\Omega \ll B_{\mathrm{rot}}/\hbar$. Consequently, the field-based universality is generally applicable to other two-component fermionic and identical bosonic species, and we verified this for two different molecular species.

Building on this microscopic control, we mapped the collisional landscape near the first FLR and demonstrated an interval in microwave coupling strength where the elastic rate coefficient approaches the unitary scattering limit, while inelastic and reactive rate coefficients remain three orders of magnitude smaller. In addition, the system is expected to be stable against three-body loss with respect to the bosonic case, an effect we will explore in a future study.

The enhanced isotropic s-wave scattering in the vicinity of the FLR holds many evaporation-friendly features. In combination, they both promise to reach deep quantum degeneracy in ultracold dipolar fermionic molecules. This sets the stage for exploring anisotropic superfluidity, dipolar polarons, quantum magnetism, and novel topological phases. Beyond ultracold molecular gases, the universal scaling we uncover may inform further dipolar interaction control strategies in hybrid atom–ion systems[69] and long-range Rydberg complexes[70].

Taken together, these results elevate the microwave shielding of molecules from an experimental stabilisation technique to a versatile interaction-engineering platform, similar to magnetic Feshbach resonances in ultracold atomic gases. Future work will extend the present formalism to include many-body effects, low-dimensional confinement geometry, and time-dependent dynamics, further broadening the horizons of strongly interacting dipolar quantum matter.

Methods

Hamiltonian

Our Hamiltonian for two dipolar molecules in a microwave field reads

$$H = \sum_{i=1,2} h_i + T + V_{\mathrm{vdW}} + V_{\mathrm{dd}}, \tag{5}$$

where $h_i = B_{\mathrm{rot}}\boldsymbol{J}^2 - \boldsymbol{d}\cdot\boldsymbol{E}$ is the single-molecule Hamiltonian (identical for both molecules), T denotes the kinetic operator for the relative motion between the two-molecule centre-of-mass frames. Here, the $\boldsymbol{J}$ and $\boldsymbol{d}$ denote the rotational angular momentum and the electric dipole moment vector of the molecule, respectively. The last two terms, $V_{\mathrm{vdW}} = -C_6/r^6$ and $V_{\mathrm{dd}} = \frac{d^2}{4\pi\epsilon_0 r^3}[\hat{\boldsymbol{e}}_{d_1}\cdot\hat{\boldsymbol{e}}_{d_2} - 3(\hat{\boldsymbol{e}}_{d_1}\cdot\hat{\boldsymbol{e}}_r)(\hat{\boldsymbol{e}}_{d_2}\cdot\hat{\boldsymbol{e}}_r)]$ describe the intermolecular van der Waals and dipole–dipole interactions, respectively, while ϵ_0 denotes the vacuum permittivity. Here, $\hat{\boldsymbol{e}}_{d_1}$, $\hat{\boldsymbol{e}}_{d_2}$ and $\hat{\boldsymbol{e}}_r$ denote the unit vector of the dipoles $\boldsymbol{d}_1$ and $\boldsymbol{d}_2$ and the intermolecular position vector $\boldsymbol{r}$, respectively. We take the van der Waals coefficient C_6 as the sum of the induction C_6^{e} and dispersion $C_6^{\mathrm{g-e}}$ terms reported previously[71].

We consider a microwave electric field $\boldsymbol{E}$

$$\boldsymbol{E} = E e^{i(k_z z-\omega t)}(\cos\xi\,\hat{\boldsymbol{e}}_1 + \sin\xi\,\hat{\boldsymbol{e}}_{-1}) + \text{ c.c.} \tag{6}$$

at a frequency $\omega \approx 2B_{\mathrm{rot}}/\hbar = \omega_{\mathrm{m}}$, near resonant with the $J = 0 \to J = 1$ transition and with a ellipticity angle ξ, where $\hat{\boldsymbol{e}}_1$ and $\hat{\boldsymbol{e}}_{-1}$ are the unit vectors of circular and anticircular field, respectively. The microwave field couples the ground molecular rotational state $|J, m_J\rangle = |0,0\rangle$ with the excited superposition state $|\xi_+\rangle \equiv \cos\xi|1,1\rangle + \sin\xi|1,-1\rangle$ depending on the elliptical angle ξ. Two dark excited states, $|1,0\rangle$ and $|\xi_-\rangle \equiv \cos\xi|1,-1\rangle - \sin\xi|1,1\rangle$, to which the microwave field can not directly drive the transition, are also taken into account. Especially, these dark states become involved in two-molecule collisions due to the dipole-dipole interaction V_{dd}. Our model neglects higher excited rotational states with $J > 1$.

In the frame co-rotating with the microwave field (defined by the unitary transformation $U = \exp(-i\omega\boldsymbol{J}^2 t/2)$, the RWA can be employed to neglect the Hamiltonian terms that contain the fast time dependence factor $\exp(\pm i2\omega t)$. As a result, the system's Hamiltonian becomes static in the corresponding interaction picture defined by $H \to U^\dagger H U$. In particular, single-molecule Hamiltonian yields two field-linked eigenstates $|+\rangle = u|0,0\rangle + v|\xi_+\rangle$ and $|-\rangle = u|\xi_+\rangle - v|0,0\rangle$ with eigenenergies $E_\pm = \hbar(\delta \pm \Omega_{\mathrm{eff}})$, where $u = -\sqrt{(1-\delta/\Omega_{\mathrm{eff}})/2}$ and $v = \sqrt{(1+\delta/\Omega_{\mathrm{eff}})/2}$. Here, $\delta = \omega_{\mathrm{m}} - \omega$ denote the detuning, $\Omega = 2dE/\sqrt{3}\hbar$ is the bare Rabi requency and $\Omega_{\mathrm{eff}} = \sqrt{\delta^2 + \Omega^2}$ the effective Rabi frequency. The energies of both dark states $|1,0\rangle$ and $|\xi_-\rangle$ are the bare detuning $\hbar\delta$ in the interaction picture. The validity of RWA requires the condition of $|\delta| \ll B_{\mathrm{rot}}/\hbar, \Omega \ll B_{\mathrm{rot}}/\hbar$.

Coupled-channel approach

The scattering problem of two field-linked molecules, governed by the Hamiltonian (5), is numerically solved in the interaction picture using the coupled-channel Schrödinger equation framework. The two-molecule internal channel states involved here are the product state in the single-molecule basis $|\nu\rangle \in \{|+\rangle, |-\rangle, |1,0\rangle, |\xi_-\rangle\} \otimes \{|+\rangle, |-\rangle, |1,0\rangle, |\xi_-\rangle\}$, yielding 16 total combinations. Through symmetrization, the 16 two-molecule basis states are classified into 10 symmetric basis states $|\nu_s\rangle \in$

$\mathcal{S}\{|+\rangle,|-\rangle,|1,0\rangle,|\xi_-\rangle\}\otimes\{|+\rangle,|-\rangle,|1,0\rangle,|\xi_-\rangle\}$ and 6 antisymmetric basis states $|\nu_a\rangle\in\mathcal{A}\{|+\rangle,|-\rangle,|1,0\rangle,|\xi_-\rangle\}\otimes\{|+\rangle,|-\rangle,|1,0\rangle,|\xi_-\rangle\}$. Here, $\mathcal{S}=(1+P)/2$ and $\mathcal{A}=(1-P)/2$ denote the symmetric and antisymmetric permutation operators, defined by the permutation P, of two molecules, respectively. The adiabatic Hamiltonian $H_{\rm ad}=\sum_{i=1,2}h_i+V_{\rm vdW}+V_{\rm dd}$ defines the interaction potentials and couplings associated with these internal states. We note that $H_{\rm ad}$ commutes with the permutation operator and the couplings between the internal states in the symmetric sector $\{|\nu_s\rangle\}$ and those in the antisymmetric sector $\{|\nu_a\rangle\}$ are zero. Consequently, $H_{\rm ad}$ can be written as $H_{\rm ad}=H_{\rm ad}^{\rm s}\oplus H_{\rm ad}^{\rm a}$, a product sum of its projections in the symmetric sector $H_{\rm ad}^{\rm s}$ and in the antisymmetric sector $H_{\rm ad}^{\rm a}$. Furthermore, three symmetric states $(|1,0\rangle|1,0\rangle,|\xi_-\rangle|\xi_-\rangle$ and $\mathcal{S}|1,0\rangle|\xi_-\rangle)$ and one antisymmetric state $(\mathcal{A}|1,0\rangle|\xi_-\rangle)$, which consist of only the dark states, are decoupled from others under RWA. These states can be removed from each basis set. As a result, the scattering problem can be studied either in the symmetric sector with 7 coupled $|\nu_s\rangle$ channels or in the antisymmetric sector with 5 coupled $|\nu_a\rangle$ channels, depending on the preparation of the incoming scattering state. In this work, we focus on the symmetric sector by considering two molecules prepared in the $|\nu_s^{\rm in}=++\rangle\equiv|+\rangle|+\rangle$ scattering state. The adiabatic interaction potentials $V^{\nu_s}(r,\theta,\phi)$ $[V^{\nu_a}(r,\theta,\phi)]$ are defined as the eigenvalues of $H_{\rm ad}^{\rm s}$ $(H_{\rm ad}^{\rm a})$ in the symmetric (antisymmetric) sectors. For instance, $V^{++}(r,\theta,\phi)$ denotes the adiabatic potential energy surface in the symmetric sector with a threshold the same as the channel energy of the $|++\rangle$ state. We note that without ellipticity ($\xi=0$ or $\pi/2$), potential surfaces $V^{\nu_s}(r,\theta,\phi)$ $[V^{\nu_a}(r,\theta,\phi)]$ become independent of the azimuthal angle ϕ. Accordingly, we omit ϕ from the notation in the main text. The anisotropic interaction potential $V^{\nu_s}(r,\theta,\phi)$ couples different partial wave basis $|lm_l\rangle$ associated with the rotation of $\boldsymbol{r}=(r,\theta,\phi)$. Accordingly, one can define a combined basis set $\{|\nu_s lm_l\rangle\}$ that includes the partial wave. The Schrödinger equation in $\{|\nu_s lm_l\rangle\}$ reads as a one-dimensional coupled-channel equation of r

$$-\frac{\hbar^2}{m}\frac{d^2}{dr^2}\psi_{\nu_s lm_l}+\sum_{\nu_s' l'm_l'}\left[H_{\rm ad}^{\rm s}+V_{\rm cen}\right]_{\nu_s lm_l}^{\nu_s' l'm_l'}\psi_{\nu_s' l'm'}=E\psi_{\nu_s lm_l},\qquad(7)$$

where $V_{\rm cen}=\hbar^2 l(l+1)/mr^2$ denotes the centrifugal interaction and m is the single-molecule mass. The partial wave adiabatic potential curve $V_{lm_l}^{\nu_s}(r)$ can be obtained by diagonalizing the matrix of resulting Hamiltonian $H_{\rm ad}^{\rm s}+V_{\rm cen}$. At large distance, the $V_{lm_l}^{\nu_s}(r)$ is determined by the dipole–dipole interaction $V_{\rm dd}$. This leads to a general asymptotic behavior $V_{lm_l}^{\nu_s}(r)\to^{r\to\infty}C_{\nu_s lm_l}/r^3+\hbar^2 l(l+1)/mr^2$, taking the diagonal element of the $V_{\rm dd}$. However, for $l=0$ the leading term is $V_{00}^{\nu_s}(r)\to^{r\to\infty}C_{\nu_s 00}/r^4$, arising from the second-order perturbation of $V_{\rm dd}$[33]. In the main text, the s- and p-wave partial wave adiabatic potential curves of $|\nu_s\rangle=|++\rangle$ are notated as $V_s^{++}(r)$ and $V_{pm_p}^{++}(r)$ with $m_p=0,\pm1$, respectively. We also refer to C_{++00} as $-C_4$ in the main text.

The one-dimensional coupled-channel equation (7) is solved by propagating the log-derivative matrix from a small intermolecular distance $r_{\rm in}$ with the absorbing boundary condition[72] to $r_{\rm out}$ at the asymptotic region, using the algorithm developed by Manolopoulos[73]. The scattering matrix S is obtained by matching the log-derivative matrix at $r_{\rm out}$ to the asymptotic scattering wavefunction. From the S matrix, one can define the partial elastic $K_{2,\nu_s^{\rm in}lm_l}^{\rm el}(E)=\frac{2g\pi\hbar}{mk}|1-S_{\nu_s^{\rm in}lm_l,\nu_s^{\rm in}lm_l}|^2$, inelastic $K_{2,\nu_s^{\rm in}lm_l}^{\rm in}(E)=\sum_{\nu_s' l'm_l'\neq\nu_s^{\rm in}lm_l}K_{2,\nu_s^{\rm in}lm_l}^{\nu_s' l'm_l'}(E)$ and reactive $K_{2,\nu_s^{\rm in}lm_l}^{\rm re}(E)=\frac{2g\pi\hbar}{mk}-\sum_{\nu_s' l'm_l'}K_{2,\nu_s^{\rm in}lm_l}^{\nu_s' l'm_l'}(E)$ scattering rates for the incoming internal state $|\nu_s^{\rm in}\rangle$ at each partial wave $|lm_l\rangle$. Here, $K_{2,\nu_s^{\rm in}lm_l}^{\nu_s' l'm_l'}(E)=\frac{2g\pi\hbar}{mk}|S_{\nu_s^{\rm in}lm_l,\nu_s' l'm_l'}|^2$, E is the collision energy with respect to the threshold of $\nu_s^{\rm in}=++$ channel and $k=\sqrt{mE}/\hbar$. Note that the emergence of reactive scattering rate $K_{2,\nu_s^{\rm in}lm_l}^{\rm re}(E)$ is due to the short-range absorbing boundary condition. The factor $g=2$ when the initial states of two molecules are identical (in all degrees of freedom, including spins), otherwise $g=1$. By collecting the contribution from all even partial waves, we define also the total elastic $K_2^{\rm el}(E)=\sum_{lm_l}K_{2,\nu_s^{\rm in}lm_l}^{\rm el}(E)+\sum_{lm_l l'm_l'\neq lm_l}K_{2,\nu_s^{\rm in}lm_l}^{\nu_s^{\rm in}l'm_l'}(E)$, inelastic $K_2^{\rm in}(E)=\sum_{\nu_s'\neq\nu_s^{\rm in}lm_l l'm_l'}K_{2,\nu_s^{\rm in}lm_l}^{\nu_s' l'm_l'}(E)$ and reactive $K_2^{\rm re}(E)=\sum_{lm_l}K_{2,\nu_s^{\rm in}lm_l}^{\rm re}(E)$ scattering rates for the incoming internal sate $|\nu_s^{\rm in}\rangle$. As $\nu_s^{\rm in}=++$ is fixed throughout this work, we remove it from the subscript for simplifying the notation. In this work, these scattering rates are calculated at various collision energies in [1, 1000] nK and are averaged according to the Fermi–Dirac distribution. The thermally averaged scattering rates are denoted with the subscript 'FD'. We define the s-wave scattering length as $a_s=lim_{k\to0}\frac{1}{ik}\frac{1-S_{\nu_s00,\nu_s00}}{1+S_{\nu_s00,\nu_s00}}$ while for the p-wave we define an energy dependent scattering length $a_{pm_p}=\frac{1}{ik}\frac{1-S_{\nu_s1m_p,\nu_s1m_p}}{1+S_{\nu_s1m_p,\nu_s1m_p}}$ with $m_p=0,\pm1$[42]. We note that both a_s and a_{pm_p} are in principle complex values. We focus on the real part of the scattering lengths, and define $\alpha_s=\mathrm{Re}(a_s)$ and $\alpha_{pm_p}(k)=\mathrm{Re}\,(a_{pm_p})(k)$. In the main text, we simply refer to α_s and α_{pm_p} as the s-wave scattering length and p-wave energy dependent scattering length, respectively.

The internal spin state

In addition to their internal rotational states, the molecules also possess internal spin states, denoted as $|\sigma_1\rangle$ and $|\sigma_2\rangle$ for the first and second components of the molecular spin mixture, respectively. For example, in case of ^{23}Na^{40}K internal spin states correspond to specific configurations of the molecular nuclear spins such as $|\sigma_1\rangle=|S=0,M_S=0,m_{i_{\rm Na}}=3/2,m_{i_{\rm K}}=-4\rangle$ and $|\sigma_2\rangle=|S=0,M_S=0,m_{i_{\rm Na}}=3/2,m_{i_{\rm K}}=-3\rangle$. Here, S and M_S denote the total electronic spin of ^{23}Na^{40}K and its projection quantum number, while $m_{i_{\rm Na}}$ and $m_{i_{\rm K}}$ are the projection quantum numbers of the individual nuclear spins of ^{23}Na and ^{40}K, respectively. Under typical experimental conditions in the presence of a magnetic field, the nuclear spin of the molecules is decoupled from other degrees of freedom and is therefore treated as a spectator in the scattering process[49,52,74,75]. For ^{23}Na^{40}K, a magnetic field of 70 G suffices[47]. That is, including the molecular spin degree of freedom does not alter the overall adiabatic Hamiltonian $H_{\rm ad}$ of the microwave field-dressed molecules. Two molecules prepared in the state $|++\rangle$, but with different spin configurations, will collide on the same $V^{++}(r,\theta,\phi)$ potential surface, which couples identically with other $V^{\nu_s}(r,\theta,\phi)$ potential surfaces associated with $H_{\rm ad}^{s}$. Nevertheless, under fermionic statistics, the spin state of the two molecules significantly affects their low-energy scattering properties. Given the above-defined mixtures, two molecules can have two intra-spin configurations, $|\sigma_1\sigma_1\rangle$ and $|\sigma_2\sigma_2\rangle$, and two inter-spin configurations $|\sigma_1\sigma_2\rangle^{\rm s}=(|\sigma_1\sigma_2\rangle+|\sigma_2\sigma_1\rangle)/\sqrt{2}$ and $|\sigma_1\sigma_2\rangle^{\rm a}=(|\sigma_1\sigma_2\rangle-|\sigma_2\sigma_1\rangle)/\sqrt{2}$. The two intra-spin configurations and inter-spin $|\sigma_1\sigma_2\rangle^{\rm s}$ state are symmetric, while the inter-spin $|\sigma_1\sigma_2\rangle^{\rm a}$ is antisymmetric. For two fermionic molecules in the $|++\rangle$ rotational state, the antisymmetry of the total wave function requires the odd partial waves $l=1,3,5,\cdots$ for the symmetric spin state, while even-partial waves $l=0,2,4,\cdots$ for the antisymmetric spin state. As a result, the lowest collisional channel is s-wave for inter-spin scattering in $|\sigma_1\sigma_2\rangle^{\rm a}$, whereas it is p-wave for intra-spin scatterings, $|\sigma_1\sigma_1\rangle$ and $|\sigma_2\sigma_2\rangle$, and for inter-spin scattering in $|\sigma_1\sigma_2\rangle^{\rm s}$, where a centrifugal barrier must be overcome.

Data availability

The data that support the findings of this study are available from the corresponding authors upon request.

Code availability

The computational codes that were used to generate the figures presented in this study are available from the corresponding authors upon request.

Received: 22 July 2025; Accepted: 26 February 2026;
Published online: 14 April 2026

References

1. Inguscio, M., Ketterle, W., & Salomon, C., editors. *Proceedings, International School of Physics "Enrico Fermi", 164th Course, "Ultracold Fermi Gases"*: Varenna, Italy, June 20-30, 2006, volume 164, Amsterdam, 2007. IOS Pr.
2. Bloch, I., Dalibard, J. & Wilhelm, Z. Many-body physics with ultracold gases. *Rev. Mod. Phys.* **80**, 885–964 (2008).
3. Ketterle, W. & Van Druten, N. J. Evaporative Cooling of Trapped Atoms. volume 37 of *Advances In* Atomic, Molecular, and Optical Physics, pages 181–236. Academic Press, 1996.
4. Chin, C., Grimm, R.Julienne, P. & Tiesinga, E. Feshbach resonances in ultracold gases. *Rev. Mod. Phys*., 82:1225–1286, Apr 2010.
5. Zwerger, W.*The BCS-BEC Crossover and the Unitary Fermi Gas*. Springer Science & Business Media, oct 2011.
6. Wenzel, M., Böttcher, F. & Schmidt, J. N. Michael Eisenmann, Tim Langen, Tilman Pfau, and Igor Ferrier-Barbut. Anisotropic superfluid behavior of a dipolar Bose-Einstein condensate. *Phys. Rev. Lett.* **121**, 030401 (2018).
7. Savary, L. & Balents, L. Quantum spin liquids: a review. *Rep. Prog. Phys.* **80**, 016502 (2016).
8. Kestner, J. P., Wang, B., Sau, J. D. & Das Sarma, S. Prediction of a gapless topological Haldane liquid phase in a one-dimensional cold polar molecular lattice. *Phys. Rev. B* **83**, 174409 (2011).
9. Chomaz, L., Ferrier-Barbut, I. & Ferlaino, F. Bruno Laburthe-Tolra, Benjamin L Lev, and Tilman Pfau. Dipolar physics: a review of experiments with magnetic quantum gases. *Rep. Prog. Phys.* **86**, 026401 (2023).
10. Carr, L. D., DeMille, D., Krems, R. V. & Ye, J. Cold and ultracold molecules: science, technology and applications. *N. J. Phys.* **11**, 055049 (2009).
11. Cooper, N. R. & Shlyapnikov, G. V. Stable topological superfluid phase of ultracold polar fermionic molecules. *Phys. Rev. Lett.* **103**, 155302 (2009).
12. Shi, T., Zhang, J.-N., Sun, C.-P. & Yi, S. Singlet and triplet Bardeen-Cooper-Schrieffer pairs in a gas of two-species fermionic polar molecules. *Phys. Rev. A* **82**, 033623 (2010).
13. Schmidt, M., Lassablière, L., Quéméner, G. & Langen, T. Self-bound dipolar droplets and supersolids in molecular Bose-Einstein condensates. *Phys. Rev. Res.* **4**, 013235 (2022).
14. SLangen, T., Valtolina, G., Wang, D. & Ye, J. Quantum state manipulation and cooling of ultracold molecules. *Nat. Phys.* **20**, 702–712 (2024).
15. Bruun, G. M. & Taylor, E. Quantum phases of a two-dimensional dipolar Fermi gas. *Phys. Rev. Lett.* **101**, 245301 (2008).
16. Iskin, M. & Sá De Melo, C. A. R. Ultracold Heteronuclear Molecules and Ferroelectric Superfluids. *Phys. Rev. Lett.* **99**, 110402 (2007).
17. Baranov, M. A., Dalmonte, M., Pupillo, G. & Zoller, P. Condensed Matter Theory of Dipolar Quantum Gases. *Chem. Rev.* **112**, 5012–5061 (2012).
18. Wu, Z., Block, J. K. & Bruun, G. M. Liquid crystal phases of two-dimensional dipolar gases and Berezinskii-Kosterlitz-Thouless melting. *Sci. Rep.* **6**, 19038 (2016).
19. Mukherjee, B. & Hutson, J. M. SU(N) symmetry with ultracold alkali dimers: Weak dependence of scattering properties on hyperfine state. *Phys. Rev. Res.* **7**, 013099 (2025).
20. Mukherjee, B., Hutson, J. M. & Hazzard, K. R. A. SU(N) magnetism with ultracold molecules. *N. J. Phys.* **27**, 013013 (2025).
21. Santos, L., Shlyapnikov, G. V., Zoller, P. & Lewenstein, M. Bose-Einstein Condensation in Trapped Dipolar Gases. *Phys. Rev. Lett.* **85**, 1791–1794 (2000).
22. Lushnikov, P. M. Collapse of Bose-Einstein condensates with dipole-dipole interactions. *Phys. Rev. A* **66**, 051601 (2002).
23. Ospelkaus, S. et al. Quantum-State Controlled Chemical Reactions of Ultracold Potassium-Rubidium Molecules. *Science* **327**, 853–857 (2010).
24. Mayle, M., Quéméner, G., Ruzic, B. P. & Bohn, J. L. Scattering of ultracold molecules in the highly resonant regime. *Phys. Rev. A* **87**, 012709 (2013).
25. Christianen, A., Zwierlein, M. W., Groenenboom, G. C. & Karman, T. Photoinduced Two-Body Loss of Ultracold Molecules. *Phys. Rev. Lett.* **123**, 123402 (2019).
26. Liu, Y. et al. Photo-excitation of long-lived transient intermediates in ultracold reactions. *Nat. Phys.* **16**, 1132–1136 (2020).
27. Gregory, P. D., Blackmore, J. A., Bromley, S. L. & Cornish, S. L. Loss of Ultracold $^{87}Rb^{133}Cs$ Molecules via Optical Excitation of Long-Lived Two-Body Collision Complexes. *Phys. Rev. Lett.* **124**, 163402 (2020).
28. Bause, R., Christianen, A., Schindewolf, A., Bloch, I. & Luo, X. Y. Ultracold Sticky Collisions: Theoretical and Experimental Status. *J. Phys. Chem. A* **127**, 729–741 (2023).
29. Park, J. J., Lu, Y. K., Jamison, A. O., Tscherbul, T. V. & Ketterle, W. A Feshbach resonance in collisions between triplet ground-state molecules. *Nature* **614**, 54–58 (2023).
30. Büchler, H. P. et al. Strongly correlated 2D quantum phases with cold polar molecules: Controlling the shape of the interaction potential. *Phys. Rev. Lett.* **98**, 060404 (2007).
31. Micheli, A., Pupillo, G., Büchler, H. P. & Zoller, P. Cold polar molecules in two-dimensional traps: Tailoring interactions with external fields for novel quantum phases. *Phys. Rev. A* **76**, 043604 (2007).
32. Huang, S.-J. et al. Field-induced long-lived supermolecules. *Phys. Rev. A* **85**, 055601 (2012).
33. Tijs, K. & Hutson, J. M. Microwave shielding of ultracold polar molecules. *Phys. Rev. Lett.* **121**, 163401 (2018).
34. Lassablière, L. & Quéméner, G. Controlling the scattering length of ultracold dipolar molecules. *Phys. Rev. Lett.* **121**, 163402 (2018).
35. Loïc, A. et al. Observation of microwave shielding of ultracold molecules. *Science* **373**, 779–782 (2021).
36. Deng, F. et al. Effective potential and superfluidity of microwave-shielded polar molecules. *Phys. Rev. Lett.* **130**, 183001 (2023).
37. Alexandr, V. A. & Bohn, J. L. Collisional dynamics of ultracold OH molecules in an electrostatic field. *Phys. Rev. A* **66**, 052718 (2002).
38. Avdeenkov, A. V. & Bohn, J. L. Linking Ultracold Polar Molecules. *Phys. Rev. Lett.* **90**, 043006 (2003).
39. Avdeenkov, A. V., Bortolotti, D. C. E. & Bohn, J. L. Field-linked states of ultracold polar molecules. *Phys. Rev. A* **69**, 012710 (2004).
40. Gorshkov, A. V. et al. Suppression of inelastic collisions between polar molecules with a repulsive shield. *Phys. Rev. Lett.* **101**, 073201 (2008).
41. Matsuda, K. et al. Resonant collisional shielding of reactive molecules using electric fields. *Science* **370**, 1324–1327 (2020).
42. Chen, X. Y. et al. Field-linked resonances of polar molecules. *Nature* **614**, 59–63 (2023).
43. Quéméner, G., Bohn, J. L. & Croft, J. F. E. Electroassociation of ultracold dipolar molecules into tetramer field-linked states. *Phys. Rev. Lett.* **131**, 043402 (2023).
44. Chen, X. Y. et al. Ultracold field-linked tetratomic molecules. *Nature* **626**, 283–287 (2024).
45. Deng, F. et al. Formation and dissociation of field-linked tetramers, May 2024. arXiv:2405.13645 [quant-ph].
46. Gu, Z. et al. Tetratomic states of microwave dressed and associated ultracold $^{23}Na^{40}K$ molecules, September 2025. arXiv:2509.23634 [cond-mat.quant-gas].
47. Schindewolf, A. et al. Evaporation of microwave-shielded polar molecules to quantum degeneracy. *Nature* **607**, 677–681 (2022).
48. Deng, F., Hu, X., Jin, W. J., Yi, S. & Shi, T. Two- and many-body physics of ultracold molecules dressed by dual microwave fields. *Nat. Commun*. *16*, 1129 (2025).
49. Karman, T. et al. Double Microwave Shielding. *PRX Quantum* **6**, 020358 (2025).

50. Bigagli, N. et al. Observation of Bose-Einstein condensation of dipolar molecules. *Nature* **631**, 289–293 (2024).
51. Shi, Z. et al. Bose-einstein condensate of ultracold sodium-rubidium molecules with tunable dipolar interactions, August 2025. arXiv:2508.20518 [cond-mat.quant-gas]..
52. Karman, T. & Hutson, J. M. Microwave shielding of ultracold polar molecules with imperfectly circular polarization. *Phys. Rev. A* **100**, 052704 (2019).
53. Dutta, J., Mukherjee, B. & Hutson, J. M. Universality in the microwave shielding of ultracold polar molecules. *Phys. Rev. Res.* **7**, 023164 (2025).
54. Karman, T., Frye, M. D., Reddel, J. D. & Hutson, J. M. Near-threshold bound states of the dipole-dipole interaction. *Phys. Rev. A* **98**, 062502 (2018).
55. Raab, P. & Friedrich, H. Quantization function for potentials with $-1/r^4$ tails. *Phys. Rev. A* **80**, 052705 (2009).
56. Idziaszek, Z., Simoni, A., Calarco, T. & Julienne, P. S. Multichannel quantum-defect theory for ultracold atom-ion collisions. *N. J. Phys.* **13**, 083005 (2011).
57. Bohn, J. L., Cavagnero, M. & Ticknor, C. Quasi-universal dipolar scattering in cold and ultracold gases. *N. J. Phys.* **11**, 055039 (2009).
58. Wang, R. R. W. & Bohn, J. L. Anisotropic thermalization of dilute dipolar gases. *Phys. Rev. A* **103**, 063320 (2021).
59. Bigagli, N. et al. Collisionally stable gas of bosonic dipolar ground-state molecules. *Nat. Phys.* **19**, 1579–1584 (2023).
60. Stevenson, I. et al. Three-body recombination of ultracold microwave-shielded polar molecules. *Phys. Rev. Lett.* **133**, 263402 (2024).
61. Yuan, W. et al. Extreme Loss Suppression and Wide Tunability of Dipolar Interactions in an Ultracold Molecular Gas, May 2025. arXiv:2505.08773 [cond-mat].
62. Esry, B. D., Greene, C. H. & Suno, H. Threshold laws for three-body recombination. *Phys. Rev. A* **65**, 010705 (2001).
63. D'Incao, J. P. Few-body physics in resonantly interacting ultracold quantum gases. *J. Phys. B: At., Mol. Optical Phys.* **51**, 043001 (2018).
64. Mukherjee, B. & Hutson, J. M. Controlling collisional loss and scattering lengths of ultracold dipolar molecules with static electric fields. *Phys. Rev. Res.* **6**, 013145 (2024).
65. Wang, R. R. W. et al. Simulations of evaporation to deep Fermi degeneracy in microwave-shielded molecules. *Phys. Rev. A* **110**, 043309 (2024).
66. Haussmann, R., Rantner, W., Cerrito, S. & Zwerger, W. Thermodynamics of the bcs-bec crossover. *Phys. Rev. A* **75**, 023610 (2007).
67. Yuan, W. et al. A planar cloverleaf antenna for circularly polarized microwave fields in atomic and molecular physics experiments. *Rev. Sci. Instrum.* **94**, 123201 (2023).
68. Zhang, S. et al. Observation of Self-Bound Droplets of Ultracold Dipolar Molecules, September 2025. arXiv:2507.15208.
69. Tomza, M. et al. Cold hybrid ion-atom systems. *Rev. Mod. Phys.* **91**, 035001 (2019).
70. Shaffer, J. P., Rittenhouse, S. T. & Sadeghpour, H. R. Ultracold Rydberg molecules. *Nat. Commun.* **9**, 1965 (2018).
71. Lepers, M., Vexiau, R., Aymar, M., Bouloufa-Maafa, N. & Dulieu, O. Long-range interactions between polar alkali-metal diatoms in external electric fields. *Phys. Rev. A* **88**, 032709 (2013).
72. Wang, G. & Quéméner, G. Tuning ultracold collisions of excited rotational dipolar molecules. *N. J. Phys.* **17**, 035015 (2015).
73. Manolopoulos, D. E. An improved log derivative method for inelastic scattering. *J. Chem. Phys.* **85**, 6425–6429 (1986).
74. Will, S. A., Park, J. W., Yan, Z. Z., Loh, H. & Zwierlein, M. W. Coherent microwave control of ultracold $^{23}Na^{40}K$ molecules. *Phys. Rev. Lett.* **116**, 225306 (2016).
75. Karman, T. & Hutson, J. M. Microwave shielding of ultracold polar molecules. *Phys. Rev. Lett.* **121**, 163401 (2018).
76. González-Martínez, M. L., Bohn, J. L. & Quéméner, G. Adimensional theory of shielding in ultracold collisions of dipolar rotors. *Phys. Rev. A* **96**, 032718 (2017).

Acknowledgements

J.-L.Li thanks Gaoren Wang for valuable discussions on the absorbing boundary condition. G.M.K. thanks P. Giannakeas for fruitful discussions during the initial stages of this study. G.M.K. was funded by the Austrian Science Fund (FWF) [10.55776/F1004]. R.A. received funding from the Austrian Academy of Science ÖAW grant No. PR1029OEAW03. A.S. acknowledges funding from the European Union's Horizon Europe research and innovation programme under grant agreement No. 101219560.

Author contributions

The theoretical calculations and their numerical implementation were performed by J.-L.L. and G.M.K. R. A. and A. S. proposed and coordinated the project. M.L. and R.A. supervised the work. M.H. carried out the initial calculations. All authors contributed to the development of the research, the interpretation of the results, and the writing of the manuscript.

Competing interests

The authors declare no competing interests.

Additional information

Supplementary information The online version contains supplementary material available at https://doi.org/10.1038/s42005-026-02578-8.

Correspondence and requests for materials should be addressed to Jing-Lun Li or Ragheed Alhyder.

Peer review information *Communications Physics* Physics thanks Tao Shi and the other, anonymous, reviewer(s) for their contribution to the peer review of this work. A peer review file is available.